Journal of Hazardous Materials 285 (2015) 173–181

Contents lists available at ScienceDirect

Journal of Hazardous Materials

journal homepage: www.elsevier.com/locate/jhazmat

Facile preparation of hierarchically porous diatomite/MFI-type zeolite composites and their performance of benzene adsorption: The effects of NaOH etching pretreatment

Wenbin Yu[a,c,d], Peng Yuan[a,d,*], Dong Liu[a,d], Liangliang Deng[a,c,d], Weiwei Yuan[a,c,d], Bo Tao[b,c], Hefa Cheng[b], Fanrong Chen[a,d]

[a] CAS Key Laboratory of Mineralogy and Metallogeny, Guangzhou Institute of Geochemistry, Chinese Academy of Sciences, Wushan, Guangzhou 510640, China
[b] State Key Laboratory of Organic Geochemistry, Guangzhou Institute of Geochemistry, Chinese Academy of Sciences, Wushan, Guangzhou 510640, China
[c] University of Chinese Academy of Sciences, Beijing 100049, China
[d] Guangdong Provincial Key Laboratory of Mineral Physics and Materials, Wushan, Guangzhou 510640, China

HIGHLIGHTS

- Novel hierarchical diatomite zeolite composites prepared by a NaOH etching method.
- NaOH etching enlarged macropores of frustule and increased coated zeolite contents.
- The composites exhibited good macro-/microporosity and high specific surface area.
- The composites exhibited excellent performance for benzene adsorption.

ARTICLE INFO

Article history:
Received 6 September 2014
Received in revised form
16 November 2014
Accepted 24 November 2014
Available online 25 November 2014

Keywords:
Diatomite
MFI-type zeolite
Composites
NaOH etching
Benzene adsorption

ABSTRACT

Hierarchically porous diatomite/MFI-type zeolite (Dt/Z) composites with excellent benzene adsorption performance were prepared. The hierarchical porosity was generated from the microporous zeolite coated at the surface of diatom frustules and from the macroporous diatomite support. A facile NaOH etching method was employed for the first time to treat the frustule support, followed by hydrothermal growth of MFI-type zeolite at the surface of frustules previously seeded with nanocrystalline silicalite-1 (Sil-1). NaOH etching enlarged the pores on diatom frustules and further increased the coated zeolite contents (W_z). The central macropore size of the diatom frustules increased from approximately 200–500 nm to 400–1000 nm after NaOH etching. The W_z could reach 61.2%, while the macroporosity of the composites was largely preserved due to more voids for zeolite coating being formed by NaOH etching. The Dt/Z composites exhibited higher benzene adsorption capacity per unit mass of zeolite and less mass transfer resistance than Sil-1, evaluated via a method of breakthrough curves. These results demonstrate that etching of a diatomite support is a facile but crucial process for the preparation of Dt/Z composites, enabling the resulting composites to become promising candidates for uses in volatile organic compounds emission control.

1. Introduction

Volatile organic compounds (VOCs) are the most common air pollutants emitted from chemical, petrochemical, pharmaceutical, building materials, and printing industries. Most VOCs are toxic or even carcinogenic (such as benzene) and are the main sources of photochemical reactions in the atmosphere leading to various environmental hazards [1,2]. Many technologies are available for VOCs control, such as adsorption [3], condensation [4], membrane separation [5], oxidation [6], and biological treatment [7], among which adsorption is the most applicable technology because of the flexibility of the system, low energy, and inexpensive operation costs [3,8].

Activated carbon has long been recognized as the most versatile adsorbent due to its low cost and excellent adsorption capacity [9]. However, several drawbacks, such as hygroscopicity, pore clogging,

* Corresponding author. Tel.: +86 20 85290341; fax: +86 20 85290341.
E-mail address: yuanpeng@gig.ac.cn (P. Yuan).

http://dx.doi.org/10.1016/j.jhazmat.2014.11.034
0304-3894/

and low thermal stability are associated with its use in adsorption processes [10]. Hence, extensive efforts have been focused on finding alternative adsorbents [11–15]. MFI-type zeolites with low Al content or purely siliceous form (silicalite-1) have been proposed as potential adsorbents due to their high hydrophobicity/organophilicity, large surface area, and superior thermal stability [16,17]. However, these zeolites possess only micropore channels (sinusoidal channels with 0.54 nm circular cross sections interconnected with straight channels with 0.51 nm × 0.57 nm elliptical cross sections [18]), resulting in both relatively slow mass transport and their high price, which is caused mainly by the need to use expensive templates during the preparation process. These limitations have greatly hindered their use in adsorption processes.

To overcome the diffusion limitation, hierarchically porous structured zeolites, which integrate at least two levels of porosity (meso-/micropores or macro-/micropores) within a single body, have been developed to improve the diffusion performance of such adsorbent. The general route for synthesizing such materials is the template-directed method. In this method, the zeolite crystals closely contact a sacrificial template (such as polystyrene beads [19], differently structured carbon materials [20–22], surfactants [23]) that is later removed by calcination or extraction to obtain a hierarchically porous structure. However, the materials synthesized by this method often exhibit inferior mechanical strength, limiting their practical application. Moreover, the removal of a large amount of template is not only a waste of resources but also harmful to the environment. Coating or supporting zeolite crystals at the surface of a permanent support to fabricate hierarchically porous structured composites (supported zeolites) is an alternative strategy to avoid the above problems. These composites can benefit in their application from both the zeolitic function (e.g., adsorption or catalytic performance) and the function of the supports (e.g., mechanical stability, pressure drop reduction, or mass transport). Various materials including porous stainless steel [24], porous glass [25], solid foam monoliths [26,27], ordered mesoporous silicates [28], and porous minerals [29–31] have been used as permanent supports. Among these materials, diatomite is a particularly attractive support [32]. Diatomite, also known as diatomaceous earth or kieselgur, is a fossil assemblage of diatom frustules, characteristics of which are highly developed porosity, and a particularly macroporous structure; thus, these materials can improve the efficiency of the mass-transport and diffusion processes [33]. Diatom frustules are mainly composed of amorphous hydrated silica ($SiO_2 \cdot nH_2O$), which is categorised as non-crystalline opal-A according to the mineralogical classification [34,35]. Composed of diatomaceous silica, which is the most abundant form of silica on earth, diatomite can also act as inexpensive nutrients for the growth of zeolites [36,37].

There have been several reports of the use of diatomite as a support for the synthesis of diatomite/zeolite composite. For example, Anderson et al. [30] synthesized a diatomite/MFI-type zeolite composite and observed a high diffusion rate of water, and Lu et al. [38] prepared a diatomite/silicalite-1 composite for the effective removal of methyl *tert*-butyl ether from a water system. However, the aforementioned composites show low specific surface area (S_{BET}, 29.2 m^2/g for Anderson et al. and 45 m^2/g for Lu et al.) and micropore volumes ($V_{micropore}$, 0.010 cm^3/g for Anderson et al. and 0.018 m^2/g for Lu et al.) due to the low amounts of zeolite coating on the diatomite (w/w, 5% for Anderson et al. and 12% for Lu et al.). To grow more zeolite crystals on diatomite, the synthesis by Anderson et al. lasted for 72 h [30]. However, the characteristic array of submicron pores and even the larger internal voids of the diatomite were blocked by the overgrowth zeolite crystals, resulting in a decrease of the diffusion channels. This is perhaps a primary reason why there has been no report on VOCs emission controlling by using diatomite/zeolite composites as adsorbents.

In this work, for the first time, we proposed a facile NaOH etching method to treat a diatomite (Dt) support, followed by hydrothermal growth of MFI-type zeolite at the surface of the etched diatom frustules previously seeded with nanocrystalline silicalite-1 (Sil-1) to prepare diatomite/MFI-type zeolite (Dt/Z) composites. The prepared Dt/Z composites possessed hierarchically porous structure, generating from the microporous zeolite coated at the surface of diatom frustules and from the macroporous diatom frustules as the support. Among the VOCs, benzene is an important chemical feedstock and gasoline ingredient. Its emissions from multiple sources (e.g., petrochemical plants, printing office, Chinese-style cooking, and the installations where benzene is used as a solvent) have to be carefully controlled, due to its proven human carcinogenicity [39,40]. Herein, benzene was used as a model pollution to evaluate the VOCs adsorption performance of the resulting composites via a method of breakthrough curves. The influences of NaOH etching on the morphology and architecture changes of diatom frustules as well as on the structure and benzene adsorption performance of the Dt/Z composites were investigated.

2. Experimental

2.1. Reagents and materials

Tetraethoxysilane (TEOS, 99%) and diallyldimethylammonium chloride (PDDA, 20 wt% in the water) were purchased from Aldrich. Tetrapropylammonium hydroxide (TPAOH, 25 wt% in the water) was obtained from Zhejiang Kente Chemical Co., Ltd. Sodium hydroxide pellets (AR Grade) were purchased from Nanjing Chemical Reagent Co., Ltd. Distilled water was used in all of the experiments. Raw diatomite was obtained from Qingshanyuan Diatomite Co., Ltd. (Jilin province, China) and purified using the sedimentation method [41]. The chemical composition (wt%) of the purified diatomite (Dt) is: SiO_2, 85.76; Al_2O_3, 5.60; Fe_2O_3, 1.74; K_2O, 0.99; CaO, 0.33; MgO, 0.01; Na_2O, 0.20; TiO_2, 0.26; ignition loss, 4.64.

2.2. NaOH etching and preparation of Dt/Z composites

In a typical etching procedure, 1 g of Dt was placed in a plastic beaker and mixed with 20 mL of pH 13.5 NaOH solution under moderate stirring. After a 72 h reaction at room temperature, the etched sample was collected by centrifugation and washed repeatedly with distilled water until achieving neutrality, dried at 80 °C overnight, and ground into a powder in a mortar. The obtained product was denoted Dt-E.

The Dt/Z composites were prepared by the following steps: an suspension of Sil-1 with an average size of 80 nm was prepared according to a previously reported procedure [42]. A layer-by-layer electrostatic assembly technique was used to perform the seeding process [43]. The Sil-1 seeded samples were denoted Dt_{seeded} or Dt-E_{seeded}. For hydrothermal growth, 0.5 g of Sil-1 seeded sample was placed at the bottom of a PTFE-lined stainless steel autoclave, and 25 mL of a clear synthesis solution (composition $25SiO_2$:3.04TPAOH:$1454H_2O$) was added such that the sample was immersed. The autoclave was then placed in an oven at 106 °C and heated for several days. This composition and temperature were chosen to reduce the self-nucleation of the reaction mixture, and thus, facilitate the crystal growth to form a coherent zeolite film at the surface of the diatom frustules [44]. After hydrothermal treatment, the as-synthesized samples were washed repeatedly, dried at 80 °C overnight, and calcined at 550 °C in air for 6 h to remove the organic template, producing the Dt(Dt-E)/Z_n composites, where *n* indicates the hydrothermal treatment time in days; for example,

Dt-E/Z_1 refers to the diatomite/MFI-type zeolite composite that was prepared by treating the Dt-E_{seeded} hydrothermally for 1 day.

2.3. Characterization methods

Various characterization techniques including X-ray powder diffraction (XRD), N_2 adsorption–desorption isotherms, Mercury intrusion porosimetry (MIP), Scanning electron microscopy (SEM), transmission electron microscopy (TEM), selected-area electron diffraction (SAED), and solid-state magic-angle-spinning (MAS) NMR were employed to monitor the Dt/Z composites preparation process. The detailed characterization procedures are stated in the Supplementary material.

2.4. Benzene adsorption tests

The benzene adsorption performance of the obtained samples was evaluated using an in-line gas chromatographic apparatus [45,46]. The detailed benzene adsorption test procedures are stated in the Supplementary material.

The benzene adsorption capacity (q, mmol/g) of the adsorbents was calculated by integrating the area above the acquired breakthrough curve after subtracting the area attributed to the system dead volume according to the following equation:

$$q = \int_{t_1}^{t_2} F[C_0 - C_{(t)}]dt \quad (1)$$

where t_1 (min) is the breakthrough time without the column, t_2 (min) is the breakthrough time for the packed column, C_0 and $C_{(t)}$ (mmol/L) represent the influent and measured effluent benzene concentrations, respectively, and F (mL/min) is the nitrogen flow rate. The system dead volume, which is the sum of volumes extraneous to the column in the flow path, was obtained by blank runs without the column.

The breakthrough curves were fitted using the Yoon and Nelson model (Eq. (2)) [47].

$$t = \tau + \frac{1}{k}\ln\frac{C_{(t)}}{C_0 - C_{(t)}} \quad (2)$$

where t (min) is the breakthrough time, τ (min^{-1}) is the time required for 50% adsorbate breakthrough (time for $C = 0.5C_0$), and k is a rate constant that depends on the diffusion characteristics of the mass transfer zone.

3. Results and discussion

3.1. Morphology and architecture changes of diatomite rendered by NaOH etching

The XRD pattern of Dt (Fig. 1a) revealed the main phase of non-crystalline opal-A with the characteristic broad peak centered at 21.8° (2θ). Quartz impurity was also observed in the Dt sample (Fig. 1a), and its content (wt%) was semi-quantitatively determined to be approximately 4%. The XRD pattern of Dt-E (Fig. 1b) was similar to that of Dt, indicating that the NaOH etching did not alter the diatomite mineral structure.

As indicated by the SEM image (Fig. 2a), the dominant diatom of the Dt sample, which is classified in the genus *Coscinodiscus* Ehrenberg (*Centrales*), is disk-shaped and has a highly developed macroporous structure. The diatom frustules are relatively uniform in diameter (20–40 μm) and thickness (1.2–1.8 μm; SEM images not shown). For comparison, diatom frustules with similar sizes and pore distribution were selected from Dt and Dt-E for analysis. Here, *Coscinodiscus* frustules with approximately 35 μm diameters

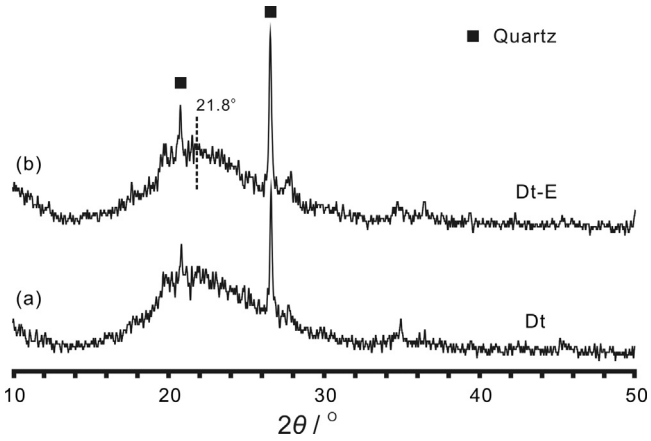

Fig. 1. XRD patterns of (a) Dt; and (b) Dt-E.

were used as an example (Fig. 2a and b). Two types of macroporous structure existed in the diatom frustule: macropores with a pore size of approximately 200–500 nm in the center of a diatom frustule (Fig. 2a_1) and others with smaller pore sizes ranging from 100 to 250 nm at the edges of the diatom frustule (Fig. 2a_2). After NaOH etching, the disk-shaped morphology of the diatom frustule was well preserved, while the edge macroporous structure of the diatom frustule disappeared, and the size of the central macropores clearly increased (Fig. 2b). The diameters of the central macropores increased to 400–1000 nm (Fig. 2b_1), and a sawtooth-shaped structure appeared at the edge of the diatom frustule (Fig. 2b_2).

The mercury intrusion results revealed three macropore size distributions in the Dt (Fig. 2c). One primary population appeared at approximately 3.20 μm, and two small populations appeared at approximately 0.22 and 0.12 μm. These populations mainly correspond to the pores formed by the stacking of diatom frustule particles and the inherent macropores of the diatom frustules, respectively. The two small populations disappeared after NaOH etching, as observed in the pore size distributions curve, and one very broad population appeared, ranging in size from 0.20 to 1.00 μm (Fig. 2c). The broad population may be due to the destruction of the pores walls thinned by NaOH etching when subjected to the pressure of mercury intrusion. This result is consistent with the above-mentioned SEM observation, indicating that NaOH etching increased the central macropore size of the diatom frustules.

The S_{BET} of Dt was 16.8 m^2/g, which decreased to 13.2 m^2/g after NaOH etching (Table 1). This decrease might have resulted from the disappearance of edge macropores, as indicated by the SEM images (Fig. 2b). The N_2 adsorption–desorption isotherm of the Dt is char-

Table 1
Porous parameters, average zeolite particle sizes, and zeolite contents of Dt, Dt-E, Sil-1, and Dt/Z composites.

Sample	S_{BET} (m^2/g)	V_{total} (cm^3/g)	$V_{micropore}$ (cm^3/g)	Zeolite crystal size[a] (nm)	W_z[b] (%)
Dt	16.8	0.042	0.006	–	–
Dt-E	13.2	0.028	0.005	–	–
Dt/Z_1	101.2	0.130	0.039	100	16.8
Dt/Z_2	130.2	0.128	0.051	150	23.0
Dt/Z_4	336.1	0.170	0.129	800	62.8
Dt-E/Z_1	88.5	0.114	0.034	100	14.8
Dt-E/Z_2	149.7	0.158	0.058	150	27.0
Dt-E/Z_4	325.4	0.176	0.125	600	61.2
Sil-1	509.8	0.720	0.196	80	100.0

[a] The value was estimated according to the SEM images.
[b] The zeolite content of the composites, W_z, was estimated form the micropore volume based on the following equation: $W_z = V_{micropore}[Dt(Dt-E)/Z_n] - V_{micropore}[Dt(Dt-E)]/V_{micropore}(Sil\text{-}1)$

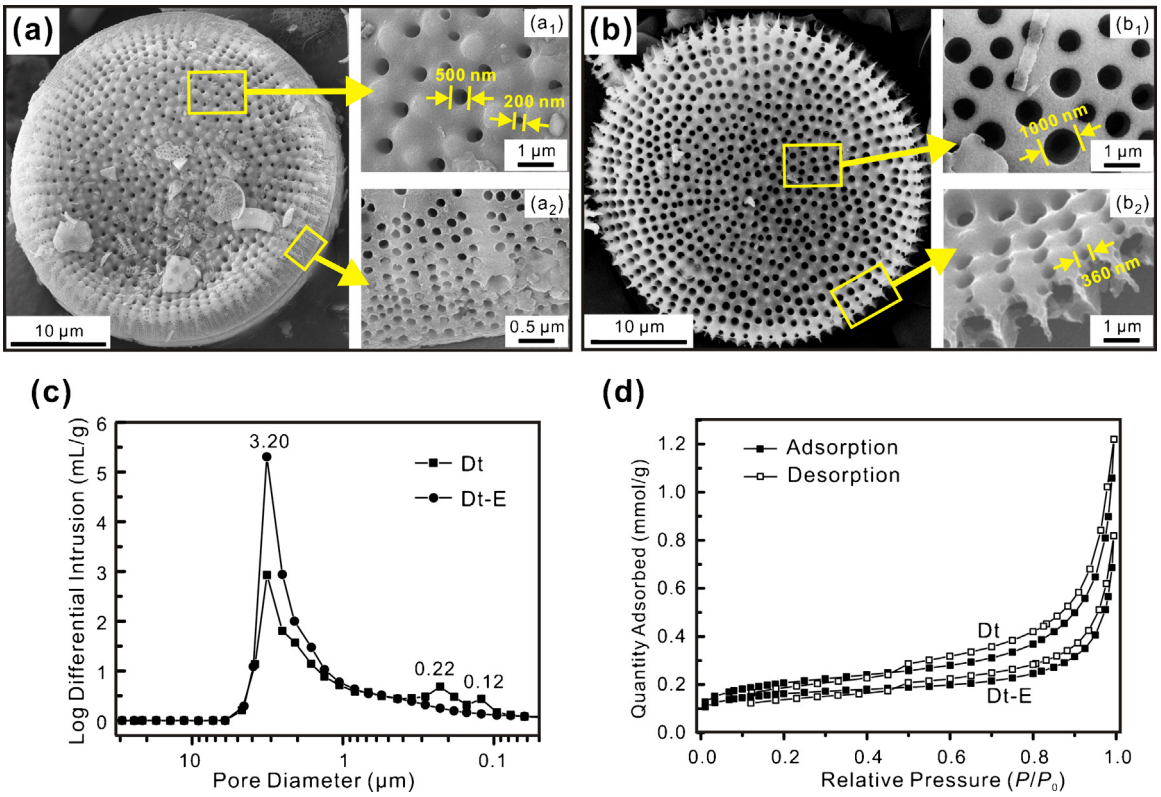

Fig. 2. (a) SEM images of Dt; (b) SEM image of Dt-E; (c) Mercury intrusion dates of Dt and Dt-E; (d) N_2 adsorption–desoption isotherms of Dt and Dt-E.

acterized as a type II isotherm with an H3 hysteresis loop (Fig. 2d), according to the IUPAC classification [48]. The hysteresis is associated with the filling and emptying of the mesopores by capillary condensation [49], indicating the existence of mesopores in the Dt. In addition, the sharp increase in the N_2 adsorbed amount near the relative pressure of one corresponds to the adsorption by macropores [50]. The entire profile of the isotherm of Dt-E did not clearly change compared with that of Dt (Fig. 2d) except for the decreased total nitrogen adsorption and weakened hysteresis, suggesting the diminishment of some mesopores on diatom frustules due to NaOH etching.

3.2. Effects of NaOH etching on the preparation of Dt/Z composites

The XRD pattern of Sil-1 is presented in Fig. 3. The diffraction pattern is consistent with the diffraction pattern for silicalite (MFI-type zeolite, Powder Diffraction File No. 44-0696) [19]. Compared with the diffraction patterns of micrometer-sized silicalite-1 [51], the diffraction lines of nano-sized Sil-1 are broadened. The newly appeared characteristic reflections of MFI-structured zeolite at 8.0°, 8.8°, 23.3°, 24.0°, and 24.4° (2θ) indicated that an MFI-type zeolite was present in the composites (Fig. 3). In addition, the intensities of the characteristic reflections of the MFI-type structure obviously increased with hydrothermal growth times (Fig. 3), indicating the growth of the nanocrystalline zeolite.

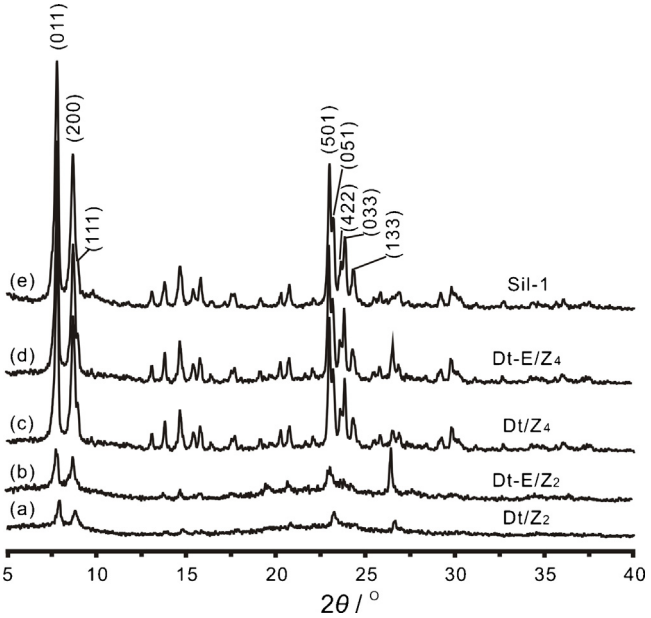

Fig. 3. XRD patterns of (a) Dt/Z_2; (b) $Dt\text{-}E/Z_2$; (c) Dt/Z_4; (d) $Dt\text{-}E/Z_4$; and (e) Sil-1.

The morphological changes occurring during the preparation steps of Dt/Z composites were revealed by SEM. As shown in the SEM image (Fig. 4a inset), Sil-1 possessed a spherical morphology with an average diameter of 80 nm. After the seeding process, nano-sized Sil-1 particles were coated homogeneously on the surface of diatom frustules as well as on the inner wall of central macropores (Fig. 4a and d). The sizes of the central macropores of both Dt_{seeded} and $Dt\text{-}E_{seeded}$ decreased by approximately 160 nm due to the nanocrystals coating the surface of the inner pore wall (Fig. 4a and d). The edge macropores of Dt_{seeded} were almost blocked by the Sil-1 particles because the diameters of the macropores were similar to the sizes of the Sil-1 particles (Fig. 4a). After hydrothermal treatment for 1 day, the nanoparticles grew only slightly (Table 1), and the macroporosity of Dt/Z_1 and $Dt\text{-}E/Z_1$ remained similar to the corresponding seeded samples (SEM images not shown). Further, hydrothermal treatment (2 days) clearly enlarged the MFI-type particles. As displayed in Fig. 4b and e, the sizes of the MFI-type particles in Dt/Z_2 and $Dt\text{-}E/Z_2$ grew to approximately 150 nm. The

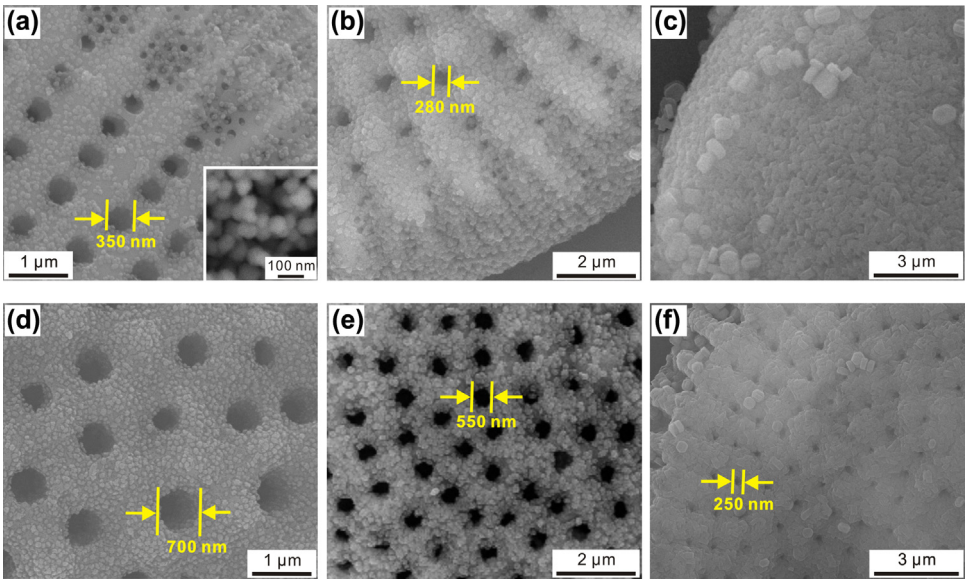

Fig. 4. SEM images of (a) Dt_{seeded} (inset: Sil-1); (b) Dt/Z_2; (c) Dt/Z_4, (d) $Dt\text{-}E_{seeded}$; (e) $Dt\text{-}E/Z_2$; and (f) $Dt\text{-}E/Z_4$.

size of the central macropores of Dt/Z_2 decreased to approximately 280 nm as the nanocrystals grew, and the macropores in the edge region were completely blocked by the grown zeolite particles (Fig. 4b). However, more macroporosity was present in sample $Dt\text{-}E/Z_2$, and the size of the macropores was as large as approximately 500 nm at this stage (Fig. 4e). Hydrothermal treatment for 4 days significantly enlarged the zeolite particles. A continuous zeolite film was formed on the surface of the diatom frustules by the intergrowth of zeolite crystals. In addition, isolated crystallites could also be observed in both Dt/Z_4 and $Dt\text{-}E/Z_4$; these crystallites had the typical hexagonal prism shape of micro-sized silicalite-1 crystals [52] (Fig. 4c and f). As shown in Fig. 4c, the macroporosity of the diatoms was completely lost for the Dt/Z_4 sample at this stage. However, both the disk morphology and the macroporosity were preserved for the $Dt\text{-}E/Z_4$ sample, although the size of macropores dramatically decreased (Fig. 4f).

A TEM image of $Dt\text{-}E/Z_2$ (Fig. 5a) reveals that the diatom frustule surface was completely and homogeneously covered with nanoparticles and that the macroporous structure of diatomite remained clearly visible. The circular streaking in the SAED pattern (inset of Fig. 5a) indicates that randomly orientated, crystalline zeolite nanocrystals coated the surface of the diatom frustules. A TEM image of $Dt\text{-}E/Z_4$ shows a dense film (dark regions) of intergrown zeolite particles (Fig. 5b). Prism-shaped crystals can be observed with clear grain boundaries on the edges of the dark regions that had been very difficult to distinguish in the SEM image (Fig. 4f). The SAED patterns of a crystal (inset of Fig. 5b) matched the SAED patterns of a previously reported MFI zeolite crystal [53], further confirming that the MFI-type zeolite was coated on the surface of the diatom frustules.

The type IV N_2 adsorption–desorption isotherms of the Dt/Z_2 and $Dt\text{-}E/Z_2$ samples were indicative of their microporosity (Fig. 6a). The steep increase at low relative pressures, corresponding to the filling of zeolitic micropores, and the hysteresis loop implied the intercrystalline mesopores space. However, a sharper increase was observed near the relative pressure of one in the adsorption isotherm of $Dt\text{-}E/Z_2$ compared with that of Dt/Z_2 (Fig. 6a), which implied that more macroporosity was present in $Dt\text{-}E/Z_2$. The N_2 adsorption–desorption isotherms of samples Dt/Z_4 and $Dt\text{-}E/Z_4$ showed that a greater quantity of N_2 was adsorbed by these samples at low relative pressures than that adsorbed by Dt/Z_2 and $Dt\text{-}E/Z_2$ (Fig. 6a), indicating that more micropores existed in Dt/Z_4 and $Dt\text{-}E/Z_4$. However, the quantity of N_2 adsorbed by Dt/Z_4 and $Dt\text{-}E/Z_4$ with the increase in relative pressure became dramatically small near the relative pressure of one (Fig. 6a) because of the loss and decrease of macroporosity in the samples Dt/Z_4 and $Dt\text{-}E/Z_4$ due to the blocking of the frustule pores, as revealed by the SEM images (Fig. 4c and f).

Fig. 6b shows the micropore and mesopore size distributions of the Dt/Z composites. The major micropore population centered

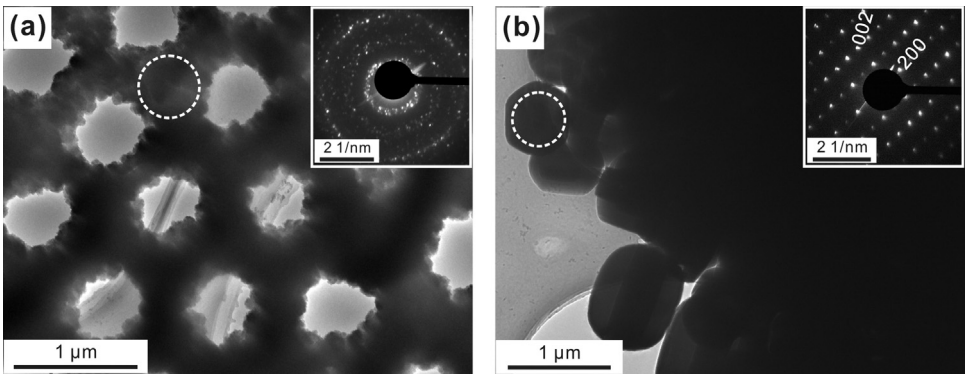

Fig. 5. TEM images of (a) $Dt\text{-}E/Z_2$ (inset: SAED pattern of the area in the dashed circles); (b) $Dt\text{-}E/Z_4$ (inset: SAED pattern of the area in the dashed circles).

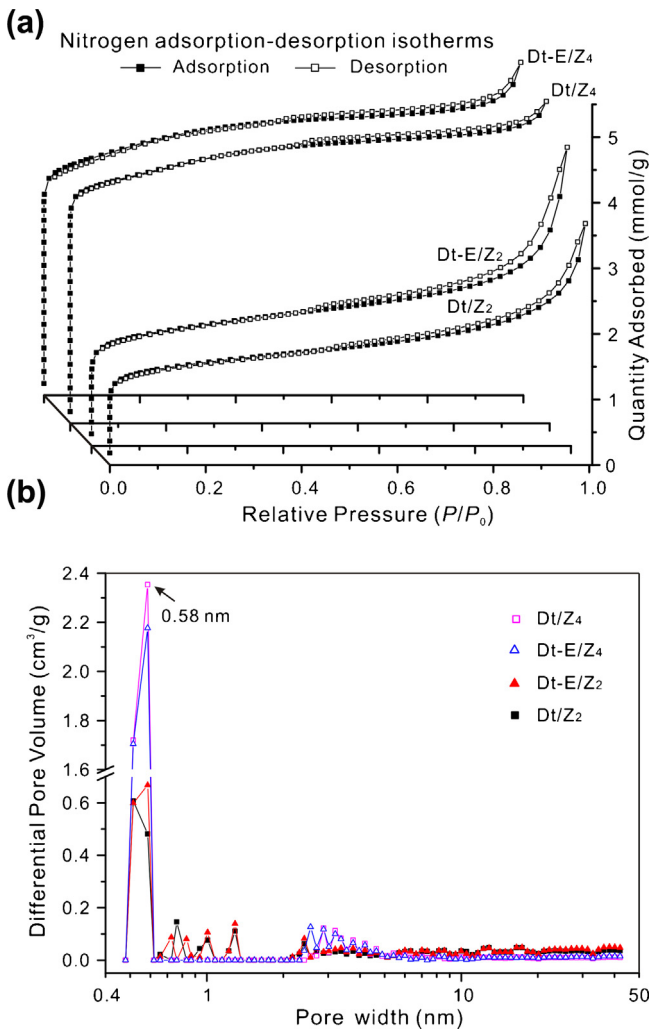

Fig. 6. (a) N_2 adsorption–desorption isotherms and (b) DFT pore size distributions of Dt/Z composites.

at approximately 0.58 nm is ascribed to the inherent micropores of MFI-type zeolite. The small micropore populations in the range of 0.60–1.50 nm for Dt/Z_2 and Dt-E/Z_2 are attributed to the stacking of smaller zeolite particles. The Dt/Z composites exhibit wide distribution of the mesopore sizes (Fig. 6b), supporting the proposal that the mesopores were derived from the intercrystalline mesopores space. It is noteworthy that Dt/Z_4 and Dt-E/Z_4 exhibited smaller mesopore size distribution range (2.00–5.00 nm) than those of Dt/Z_2 and Dt-E/Z_2 (2.00–5.00 nm and 5.00–20.00 nm). This result is due to the diminishment of intercrystalline mesopores space as the growth of zeolite crystals.

The S_{BET} and $V_{micropore}$ values of all the Dt/Z composites were significantly higher than those of the corresponding supports (Dt and Dt-E) (Table 1) due to the introduction of micropore in the composites by zeolite. Note that the S_{BET} and $V_{micropore}$ of Dt-E/Z_4 was as high as 325.4 m^2/g and 0.125 cm^3/g, respectively (Table 1), which was 6.2 and 6.9 times larger than those of the diatomite/silicalite-1 composite prepared by Lu et al. (S_{BET}, 45 m^2/g and $V_{micropore}$, 0.018 cm^3/g) [38]. The amount of zeolite coated at the surface of the etched diatom frustules for Dt-E/Z_4 (zeolite content, W_z, %) could reach 61.2% [38] (Table 1), while the macroporosity was largely preserved (Fig. 4f). This result was due to the availability of more voids for zeolite coating being formed by NaOH etching. Moreover, as shown in Table 1, the balance of zeolite content versus pore volume of the composites could be controlled by simply adjusting the time of hydrothermal growth.

^{29}Si MAS NMR spectra of the Dt-E/Z composites with the lowest (Dt-E/Z_1) and highest zeolite contents (Dt-E/Z_4) (Table 1), respectively, were compared with those of Dt and Sil-1 (Fig. 7). As shown in Fig. 7a, three peaks were observed at −112.04 ppm, −102.68 ppm, and −92.07 ppm in the ^{29}Si MAS NMR spectrum of Dt, which can be assigned to the siloxane bridge (Q^4 silicon, i.e., $Si(OSi)_4$), single silanols (Q^3, $Si(OSi)_3(OH)$), and germinal silanol (Q^2, $Si(OSi)_2(OH)_2$) of diatomaceous silica, respectively [33]. For Sil-1, two resonances with chemical shifts of −101.61(I) and −113.80(II) were observed (Fig. 7b) and were attributed to Q^3 silicons(I) and Q^4 silicons(II), respectively. The Q^4 resonance envelope sharpens, and a fine structure resulting from the 24 crystallographically inequivalent sites for Si in the framework was visible [54,55]. Seven Gaussian-shaped peaks could be distinguished by curve-fitting in the chemical shift range of the Q^4 silicons(II) (Fig. 7b), which are most likely attributable to seven different crystallographic sites for Si in the Sil-1 framework [55]. The Q^4 and Q^3 peaks in the ^{29}Si MAS NMR spectra of Sil-1 were sharper than those of Dt due to the higher degree of crystallinity of Sil-1 than that of Dt. In the ^{29}Si MAS NMR spectra of Dt-E/Z_1 and Dt-E/Z_4, the resonances at approximately −112.00 ppm became more intense than that of Dt with the increase of zeolite contents in the composites (Fig. 7c and d). This result occurred because these resonances contributed to the Q^4 silicons of both the diatomaceous silica and the MFI-type zeolite. The exact position, relative area, and assignment of each chemical shift signal of Dt-E/Z_1 and Dt-E/Z_4 are listed in Supplementary Table S1. The fractional populations of MFI-type zeolite (W_z', %) were 15.3% and 67.1% in Dt-E/Z_1 and Dt-E/Z_4, respectively, calculated using the equation $W_z' = (A(Q^4)+A(Q^3))_{zeolite}/((A(Q^4)+A(Q^3))_{zeolite}+(A(Q^4)+A(Q^3)+A(Q^2))_{diatomite})$, where A is the peak area of the Q^i group. This result was similar to the above-mentioned values calculated using the micropore volumes (Table 1), confirming the zeolite contents in the composites.

3.3. Performance of Dt/Z composites for benzene adsorption

The breakthrough measurement is a direct method designed to clarify the dynamic adsorption performance of VOCs at low concentration [11,56]. Fig. 8 presents the breakthrough curves of benzene on different adsorbents. The q values of Dt, Dt-E/Z_1, Dt-E/Z_2, Dt-E/Z_4, and Sil-1, were 0.087, 0.238, 0.308, 0.649, and 1.034 mmol/g (Table 2), respectively, which followed the same order as $V_{micropore}$ of the adsorbents (Table 1). This result revealed that the presence of micropores in the adsorbents was an important parameter for the adsorption of VOCs at low concentrations, which is in good accord with previous reports in the literature [56]. However, the q value of Dt-E/Z_1 (0.238 mmol/g) was larger than that of Dt/Z_2 (0.216 mmol/g), even though $V_{micropore}$ of Dt-E/Z_1 (0.114 cm^3/g) was smaller than that of Dt/Z_2 (0.128 cm^3/g).

Table 2
Adsorption capacity (q) and Yoon and Nelson equation parameters for benzene adsorption on various adsorbents.

Samples	Adsorption capacity		Yoon and Nelson parameters		
	q (mmol/g)	q_s(mmol/g)	τ (min)	k	R^2
Dt	0.087	–	13	0.170	0.985
Dt/Z_2	0.216	0.939	33	0.071	0.972
Dt-E/Z_1	0.238	1.608	42	0.120	0.982
Dt-E/Z_2	0.308	1.141	55	0.107	0.993
Dt-E/Z_4	0.649	1.060	125	0.052	0.991
Sil-1	1.034	1.034	201	0.035	0.977

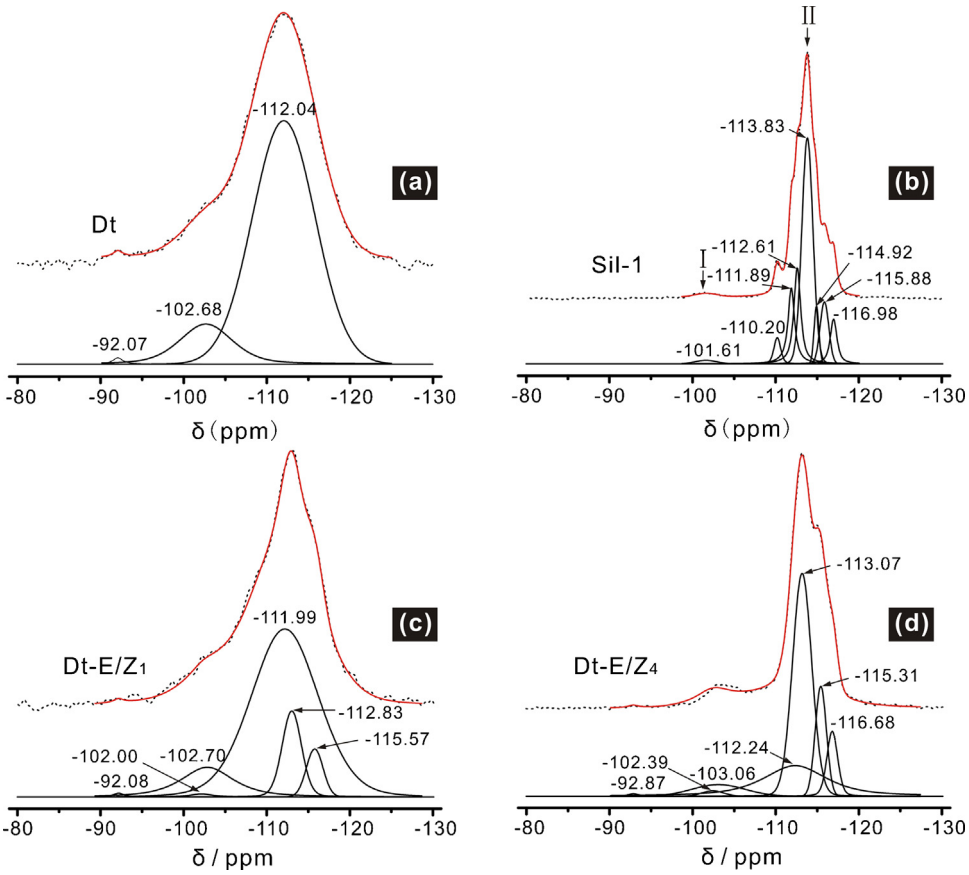

Fig. 7. ^{29}Si MAS NMR spectra of (a) Dt; (b) Sil-1; (c) Dt-E/Z_1; and (d) Dt-E/Z_4 (dotted lines for experimental and solid lines for simulated).

To compare the benzene adsorption efficiency of the Dt/Z composites with pure zeolite, the adsorption capacity normalized to the actual zeolite content, q_s, was calculated based on the values of W_z (Table 1) and q (Table 2). The contribution from the diatomite support (Dt or Dt-E) to the q_s values of the Dt/Z composites was overlooked here. The reasons were as follows: (i) the surface of the diatomite support was covered by a layer of zeolite particles or by a continuous zeolite film (as shown by SEM and TEM results); thus, it is difficult for benzene molecule to reach the surface adsorption site of diatomite; (ii) the benzene adsorption on diatomite was very minor relative to that on zeolite (Table 2). As shown in Table 2, all the Dt-E/Z composites exhibited higher q_s value than Sil-1, indicating that the Dt-E support increased the adsorption efficiency of zeolite. This result is suggested to be due to the zeolite particles coated on the surface of the etched diatom frustules obtaining better dispersion than pure microporous Sil-1. Compared with Dt-E/Z_2 and Dt-E/Z_4, Dt-E/Z_1 possessed the largest q_s value (1.608 mmol/g), which was 1.6 times that of Sil-1 (Table 2). This result most likely occurred because the zeolite particles in Dt-E/Z_1 had the largest external surface area due to their having the smallest particle size (Table 1), leading to the highest adsorption capacity per unit mass of zeolite [52]. Note that the q_s value of Dt-E/Z_2 was 22.5% greater than that of Dt/Z_2 (Table 2). Because the size of the zeolite particles in Dt-E/Z_2 was similar to that in Dt/Z_2 (Fig. 5b and e), this higher q_s was attributed to the preservation of more macroporosity in the Dt-E/Z_2 sample due to the support Dt-E having more voids available for zeolite coating after NaOH etching. Therefore, the reason why Dt-E/Z_1 exhibited a larger q value than Dt/Z_2 was proposed to be due to more macroporosity and smaller zeolite crystal size of Dt-E/Z_1.

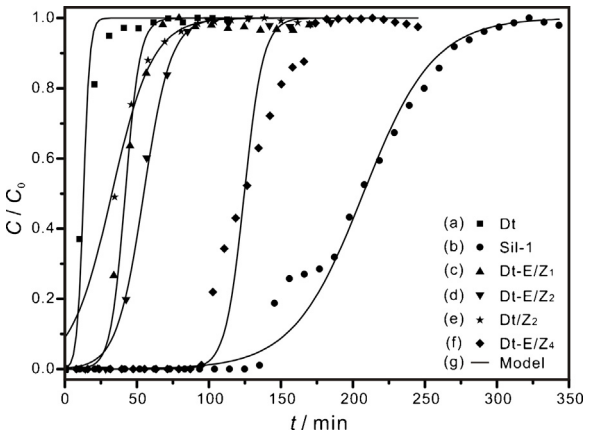

Fig. 8. Breakthrough curves and mathematic models for (a) Dt; (b) Sil-1; (c) Dt-E/Z_1; (d) Dt-E/Z_2; (e) Dt/Z_2; and (f) Dt-E/Z_4 (normalized to 0.2 g solid) at 25 °C. Dry nitrogen with benzene vapor (C_0 = 1.51 mmol/L, P/P_0 = 0.27) was passed through the column at 1.00 mL/min during sorption.

All of the post-breakthrough curves of the Dt/Z composites for benzene adsorption increased more rapidly than that of Sil-1 (Fig. 8), indicating less diffusion resistance in the Dt/Z composites during the adsorption process [15,57]. This result was due to the macroporosity of the Dt/Z composites introduced by the diatomite supports facilitating the fast diffusion and transport of gas. This finding was further confirmed by the larger rate constants (k) for the Dt/Z composites compared with that for Sil-1 (Table 2). The rate constant k for benzene adsorption in Dt-E/Z_2 was larger than that in Dt/Z_2 (Table 2), indicating less diffusion resistance in Dt-E/Z_2. This result was due to the presence of more macroporosity in Dt-E/Z_2, as already indicated by the SEM observations (Fig. 4b

and e). These results indicated that enlargement of the pores on diatomite support through NaOH etching could improve the benzene adsorption performance of Dt/Z composites. The prepared Dt/Z composites exhibited higher benzene adsorption capacity per unit mass of zeolite and less mass transfer resistance than Sil-1.

4. Conclusions

In this study, diatomite/MFI-type zeolite composites with high and hierarchical porosity were prepared by a facile method. For the first time, a NaOH etching method was proposed to treat the diatomite support, followed by hydrothermal growth of MFI-type zeolite at the surface of the etched diatom frustules previously seeded with nanocrystalline silicalite-1. NaOH etching yielded dual effects on optimising the porosity parameters of the Dt/Z composites: (i) more of the support macroporosity was preserved; (ii) substantial microporosity was introduced via a well-distributed coating of zeolite without blocking the macropores in the frustules due to the enlargement of the pores on frustules by etching. The breakthrough curves results indicated that the prepared Dt/Z composites exhibited higher benzene adsorption capacity per unit mass of zeolite and less mass transfer resistance than pure microporous nanocrystalline silicalite-1. With excellent benzene adsorption performance, the hierarchically porous diatomite/MFI-type zeolite composites can be regarded as a good benzene adsorbent, but further investigations concerning adsorption of other VOCs for emission control require to be performed.

Acknowledgments

This work was supported by National Key Technology Research and Development Program of the Ministry of Science and Technology of China (Grant No. 2013BAC01B02), Team Project of Natural Science Foundation of Guangdong Province, China (Grant No. S2013030014241) National Natural Science Foundation of China (Grant No. 41202024), and the Science and Technology Program of Guangzhou, China. This is a contribution (No. IS-1988) from GIGCAS.

Appendix A. Supplementary data

Supplementary data associated with this article can be found, in the online version, at http://dx.doi.org/10.1016/j.jhazmat.2014.11.034.

References

[1] H. Einaga, S. Futamura, T. Ibusuki, Complete oxidation of benzene in gas phase by platinized titania photocatalysts, Environ. Sci. Technol. 35 (2001) 1880–1884.
[2] D.P. Serrano, G. Calleja, J.A. Botas, F.J. Gutierrez, Adsorption and hydrophobic properties of mesostructured MCM-41 and SBA-15 materials for volatile organic compound removal, Ind. Eng. Chem. Res. 43 (2004) 7010–7018.
[3] F.J. Ma, S.X. Liu, D.D. Liang, G.J. Ren, F. Wei, Y.G. Chen, Z.M. Su, Adsorption of volatile organic compounds in porous metal–organic frameworks functionalized by polyoxometalates, J. Solid State Chem. 184 (2011) 3034–3039.
[4] P. Dwivedi, V. Gaur, A. Sharma, N. Verma, Comparative study of removal of volatile organic compounds by cryogenic condensation and adsorption by activated carbon fiber, Sep. Purif. Technol. 39 (2004) 23–37.
[5] S. Liu, W. Teo, X. Tan, K. Li, Preparation of $PDMS^{vi}$–Al_2O_3 composite hollow fibre membranes for VOC recovery from waste gas streams, Sep. Purif. Technol. 46 (2005) 110–117.
[6] S. Wang, H. Ang, M.O. Tade, Volatile organic compounds in indoor environment and photocatalytic oxidation: state of the art, Environ. Int. 33 (2007) 694–705.
[7] L. Li, S. Wang, Q. Feng, J. Liu, Removal of *o*-xylene from off-gas by a combination of bioreactor and adsorption, Asia-Pac. J. Chem. Eng. 3 (2008) 489–496.
[8] H. Wang, M. Tang, K. Zhang, D. Cai, W. Huang, R. Chen, C. Yu, Functionalized hollow siliceous spheres for VOCs removal with high efficiency and stability, J. Hazard. Mater. 268 (2014) 115–123.
[9] N. Mohan, G. Kannan, S. Upendra, R. Subha, N. Kumar, Breakthrough of toluene vapours in granular activated carbon filled packed bed reactor, J. Hazard. Mater. 168 (2009) 777–781.
[10] X. Zhao, Q. Ma, G. Lu, VOC removal: comparison of MCM-41 with hydrophobic zeolites and activated carbon, Energy Fuels 12 (1998) 1051–1054.
[11] B. Dou, J. Li, Y. Wang, H. Wang, C. Ma, Z. Hao, Adsorption and desorption performance of benzene over hierarchically structured carbon–silica aerogel composites, J. Hazard. Mater. 196 (2011) 194–200.
[12] Q. Hu, B.J. Dou, H. Tian, J.J. Li, P. Li, Z.P. Hao, Mesoporous silicalite-1 nanospheres and their properties of adsorption and hydrophobicity, Microporous Mesoporous Mater. 129 (2010) 30–36.
[13] P. Huttenloch, K.E. Roehl, K. Czurda, Sorption of nonpolar aromatic contaminants by chlorosilane surface modified natural minerals, Environ. Sci. Technol. 35 (2001) 4260–4264.
[14] F. Qu, L. Zhu, K. Yang, Adsorption behaviors of volatile organic compounds (VOCs) on porous clay heterostructures (PCH), J. Hazard. Mater. 170 (2009) 7–12.
[15] Q. Hu, J.J. Li, Z.P. Hao, L.D. Li, S.Z. Qiao, Dynamic adsorption of volatile organic compounds on organofunctionalized SBA-15 materials, Chem. Eng. J. 149 (2009) 281–288.
[16] D. Olson, G. Kokotailo, S. Lawton, W. Meier, Crystal structure and structure-related properties of ZSM-5, J. Phys. Chem. 85 (1981) 2238–2243.
[17] K. Zhang, R.P. Lively, J.D. Noel, M.E. Dose, B.A. McCool, R.R. Chance, W.J. Koros, Adsorption of water and ethanol in MFI-type zeolites, Langmuir 28 (2012) 8664–8673.
[18] G. Xomeritakis, M. Tsapatsis, Permeation of aromatic isomer vapors through oriented MFI-type membranes made by secondary growth, Chem. Mater. 11 (1999) 875–878.
[19] B.T. Holland, L. Abrams, A. Stein, Dual templating of macroporous silicates with zeolitic microporous frameworks, J. Am. Chem. Soc. 121 (1999) 4308–4309.
[20] J. Garcıa-Martınez, D. Cazorla-Amorós, A. Linares-Solano, Y. Lin, Synthesis and characterisation of MFI-type zeolites supported on carbon materials, Microporous Mesoporous Mater. 42 (2001) 255–268.
[21] I. Schmidt, A. Boisen, E. Gustavsson, K. Ståhl, S. Pehrson, S. Dahl, A. Carlsson, C.J. Jacobsen, Carbon nanotube templated growth of mesoporous zeolite single crystals, Chem. Mater. 13 (2001) 4416–4418.
[22] H.S. Cho, R. Ryoo, Synthesis of ordered mesoporous MFI zeolite using CMK carbon templates, Microporous Mesoporous Mater. 151 (2012) 107–112.
[23] F.S. Xiao, L. Wang, C. Yin, K. Lin, Y. Di, J. Li, R. Xu, D.S. Su, R. Schlögl, T. Yokoi, Catalytic properties of hierarchical mesoporous zeolites templated with a mixture of small organic ammonium salts and mesoscale cationic polymers, Angew. Chem. 118 (2006) 3162–3165.
[24] S.M. Holmes, C. Markert, R.J. Plaisted, J.O. Forrest, J.R. Agger, M.W. Anderson, C.S. Cundy, J. Dwyer, A novel method for the growth of silicalite membranes on stainless steel supports, Chem. Mater. 11 (1999) 3329–3332.
[25] B. Louis, F. Ocampo, H.S. Yun, J.P. Tessonnier, M.M. Pereira, Hierarchical pore ZSM-5 zeolite structures: from micro- to macro-engineering of structured catalysts, Chem. Eng. J. 161 (2010) 397–402.
[26] M.V. Twigg, J.T. Richardson, Fundamentals and applications of structured ceramic foam catalysts, Ind. Eng. Chem. Res. 46 (2007) 4166–4177.
[27] D. Edouard, M. Lacroix, C.P. Huu, F. Luck, Pressure drop modeling on SOLID foam: state-of-the art correlation, Chem. Eng. J. 144 (2008) 299–311.
[28] Q. Hu, J. Li, S. Qiao, Z. Hao, H. Tian, C. Ma, C. He, Synthesis and hydrophobic adsorption properties of microporous/mesoporous hybrid materials, J. Hazard. Mater. 164 (2009) 1205–1212.
[29] Q. Tan, X. Bao, T. Song, Y. Fan, G. Shi, B. Shen, C. Liu, X. Gao, Synthesis characterization, and catalytic properties of hydrothermally stable macro–meso–micro-porous composite materials synthesized via in situ assembly of preformed zeolite Y nanoclusters on kaolin, J. Catal. 251 (2007) 69–79.
[30] M.W. Anderson, S.M. Holmes, N. Hanif, C.S. Cundy, Hierarchical pore structures through diatom zeolitization, Angew. Chem. Int. Ed. 39 (2000) 2707–2710.
[31] M.W. Anderson, S.M. Holmes, R. Mann, P. Foran, C.S. Cundy, Zeolitisation of diatoms, J. Nanosci. Nanotech. 5 (2005) 92–95.
[32] P. Yuan, D. Liu, M.D. Fan, D. Yang, R.L. Zhu, F. Ge, J.X. Zhu, H.P. He, Removal of hexavalent chromium [Cr(VI)] from aqueous solutions by the diatomite-supported/unsupported magnetite nanoparticles, J. Hazard. Mater. 173 (2010) 614–621.
[33] P. Yuan, D. Liu, D.Y. Tan, K.K. Liu, H.G. Yu, Y.H. Zhong, A.H. Yuan, W.B. Yu, H.P. He, Surface silylation of mesoporous/macroporous diatomite (diatomaceous earth) and its function in Cu(II) adsorption: the effects of heating pretreatment, Microporous Mesoporous Mater. 170 (2013) 9–19.
[34] E. Stoermer, J. Smol, The Diatoms: Applications for the Environmental and Earth Sciences, Cambridge University Press, Cambridge, 2001.
[35] D. Losic, J.G. Mitchell, N.H. Voelcker, Diatomaceous lessons in nanotechnology and advanced materials, Adv. Mater. 21 (2009) 2947–2958.
[36] L.H. Chen, X.Y. Li, J.C. Rooke, Y.H. Zhang, X.Y. Yang, Y. Tang, F.S. Xiao, B.L. Su, Hierarchically structured zeolites: synthesis, mass transport properties and applications, J. Mater. Chem. 22 (2012) 17381–17403.
[37] A. Chaisena, K. Rangsriwatananon, Synthesis of sodium zeolites from natural and modified diatomite, Mater. Lett. 59 (2005) 1474–1479.

[38] J. Lu, F. Xu, W. Cai, Adsorption of MTBE on nano zeolite composites of selective supports, Microporous Mesoporous Mater. 108 (2008) 50–55.
[39] L. Zhong, M.S. Goldberg, M.-É. Parent, J.A. Hanley, Risk of developing lung cancer in relation to exposure to fumes from Chinese-style cooking, Scand. J. Work Environ. Health 25 (1999) 309–316.
[40] H. Einaga, S. Futamura, T. Ibusuki, Complete oxidation of benzene in gas phase by platinized titania photocatalysts, Environ. Sci. Technol. 35 (2001) 1880–1884.
[41] P. Yuan, D. Yang, Z.Y. Lin, H.P. He, X.Y. Wen, L.J. Wang, F. Deng, Influences of pretreatment temperature on the surface silylation of diatomaceous amorphous silica with trimethylchlorosilane, J. Non-Cryst. Solids 352 (2006) 3762–3771.
[42] A.E. Persson, B.J. Schoeman, J. Sterte, J.E. Otterstedt, The synthesis of discrete colloidal particles of TPA-silicalite-1, Zeolites 14 (1994) 557–567.
[43] Y. Wang, Y. Tang, X. Wang, A. Dong, W. Shan, Z. Gao, Fabrication of hierarchically structured zeolites through layer-by-layer assembly of zeolite nanocrystals on diatom templates, Chem. Lett. 30 (2001) 1118–1119.
[44] C. Algieri, G. Golemme, S. Kallus, J. Ramsay, Preparation of thin supported MFI membranes by in situ nucleation and secondary growth, Microporous Mesoporous Mater. 47 (2001) 127–134.
[45] H. Cheng, M. Reinhard, In-line gas chromatographic apparatus for measuring the hydrophobic micropore volume (HMV) and contaminant transformation in mineral micropores, J. Hazard. Mater. 179 (2010) 596–603.
[46] H. Cheng, M. Reinhard, Measuring hydrophobic micropore volumes in geosorbents from trichloroethylene desorption data, Environ. Sci. Technol. 40 (2006) 3595–3602.
[47] Y.H. Yoon, Application of gas adsorption kinetics I. A theoretical model for respirator cartridge service life, J. Am. Ind. Hyg. Assoc. 45 (1984) 509–516.
[48] S, K. Gregg, A.S.W. Sing, Surface Area and Porosity, Academic Press Inc. Ltd., London, 1982.
[49] P. Yuan, M. Fan, D. Yang, H. He, D. Liu, A. Yuan, J. Zhu, T. Chen, Montmorillonite-supported magnetite nanoparticles for the removal of hexavalent chromium Cr(VI) from aqueous solutions, J. Hazard. Mater. 166 (2009) 821–829.
[50] D. Liu, P. Yuan, D. Tan, H. Liu, T. Wang, M. Fan, J. Zhu, H. He, Facile preparation of hierarchically porous carbon using diatomite as both template and catalyst and methylene blue adsorption of carbon products, J. Colloid Interface Sci. 388 (2012) 176–184.
[51] E.M. Flanigen, J. Bennett, R. Grose, J. Cohen, R. Patton, R. Kirchner, Silicalite, a new hydrophobic crystalline silica molecular sieve, Nature 271 (1978) 512–516.
[52] W. Song, R. Justice, C. Jones, V. Grassian, S. Larsen, Size-dependent properties of nanocrystalline silicalite synthesized with systematically varied crystal sizes, Langmuir 20 (2004) 4696–4702.
[53] G. Bonilla, I. Díaz, M. Tsapatsis, H.-K. Jeong, Y. Lee, D.G. Vlachos, Zeolite (MFI) crystal morphology control using organic structure-directing agents, Chem. Mater. 16 (2004) 5697–5705.
[54] R. Ravishankar, C. Kirschhock, B.J. Schoeman, P. Vanoppen, P.J. Grobet, S. Storck, W.F. Maier, Johan A. Martens, F.C. De Schryver, P.A. Jacobs, Physicochemical characterization of silicalite-1 nanophase material, J. Phys. Chem. B 102 (1998) 2633–2639.
[55] C. Fyfe, G. Gobbi, J. Klinowski, J. Thomas, S. Ramdas, Resolving crystallographically distinct tetrahedral sites in silicalite and ZSM-5 by solid-state NMR, Nature 296 (1982) 530–533.
[56] K. Kosuge, S. Kubo, N. Kikukawa, M. Takemori, Effect of pore structure in mesoporous silicas on VOC dynamic adsorption/desorption performance, Langmuir 23 (2007) 3095–3102.
[57] Z.H. Huang, F. Kang, K.M. Liang, J. Hao, Breakthrough of methyethylketone and benzene vapors in activated carbon fiber beds, J. Hazard. Mater. 98 (2003) 107–115.